# Propulsión bidireccional de nadadores de remo flexible

## Bidirectional propulsion of flexible oar swimmers

Luis Felipe Córdoba-Ramírez[1]

*Fecha de recepción: 10 de abril, 2025*
*Fecha de aprobación: 23 de julio, 2025*

Córdoba-Ramírez, L.F. Propulsión bidireccional de nadadores de remo flexible. *Tecnología en Marcha*. Vol. 39 Nº 1. Enero-Marzo, 2026. Pág. 29-40.

https://doi.org/10.18845/tm.v39i1.7872

1 Instituto Tecnológico de Costa Rica. Costa Rica.
lfcordoba@itcr.ac.cr
https://orcid.org/0000-0003-2345-1528

## Palabras clave

Micronadadores; bidireccionalidad; nadadores remo flexible; bajo números de Reynolds; locomoción.

## Resumen

La capacidad de controlar micronadadores en el régimen de bajo números de Reynolds puede permitir el acceso a regiones del cuerpo previamente inalcanzables para aplicaciones biomédicas como la administración de fármacos dirigidos y la microcirugía. Los nadadores de remos flexibles pueden generar propulsión mediante la oscilación de estructuras elásticas pasivas. Sin embargo, la bidireccionalidad no se ha demostrado previamente de forma experimental con nadadores de remo flexible. La incapacidad de moverse hacia atrás limita la capacidad de navegación de los micronadadores de remo flexible, especialmente en entornos altamente confinados en los que girar es difícil o inviable. En este estudio, demostramos experimentalmente que la propulsión bidireccional de los nadadores de remos flexibles puede introducirse incorporando un perfil intrínsecamente curvado que se acciona transversalmente en un extremo del nadador. Demostramos que los nadadores intrínsecamente curvados son capaces de una propulsión bidireccional positiva, negativa y dependiente de la frecuencia, lo que podría utilizarse en entornos muy confinados en los que el giro es difícil o inviable. En última instancia, con la capacidad de lograr la propulsión bidireccional, prevemos que el robot intrínsecamente curvado puede realizar una nueva clase de micronadador que puede abordar una amplia gama de necesidades clínicas no satisfechas.

## Keywords

Microswimmers; bidirectionality; flexible oar swimmers; low Reynolds numbers; locomotion.

## Abstract

The ability to control microswimmers in the low Reynold's regime can enable access to previously unreachable regions in the body for biomedical applications such as targeted drug delivery and microsurgery. Flexible oar swimmers can generate propulsion by oscillating passive elastic structures. However, bidirectionality has not been previously experimentally demonstrated with flexible oar swimmers. The inability to move backward limits the navigation capabilities of flexible oar microswimmers, especially in highly confined environments where turning is challenging or infeasible. Here, we experimentally demonstrated that bidirectional propulsion of flexible oar swimmers can be introduced by incorporating an intrinsically-curved profile that is transversely actuated at one end of the swimmer. We show that the intrinsically curved swimmers are capable of positive, negative, and frequency-dependent bidirectional propulsion which could be utilized in highly confined environments where turning is challenging or infeasible. Ultimately, with the ability to achieve bidirectional propulsion, we envision that the intrinsically curved robot can realize a new class of microswimmer that can address a broad range of unmet clinical needs.

## Introduction

Locomotion at the microscale is crucial to an organism's survival [1] and is related to its ability to find food, reproduce, and colonize new environments [2]. The ability of microorganisms to move in the low Reynold's regime has motivated the development of artificial microscale swimmers [3]–[6], driven by biomedical applications such as targeted drug delivery and microsurgery [7]–[13]

and pipe exploration in viscous fluids or confined spaces [14], [15]. However, the microscale motion occurs at low Reynolds (Re) number environments where viscous forces dominate over inertial forces and where locomotion must incorporate nonreciprocal motions [16], [17].

Swimming mechanisms for low Re locomotion include the “corkscrew,” “three-link,” “three-linked sphere,” and “flexible oar.” The corkscrew and flexible oar methods can be implemented with a single actuation. Corkscrew swimmers consist of rigid helical structures driven by rotation to move in a manner similar to the motions of *Escherichia coli* (*E. coli*). Flexible oar swimmers, on the other hand, consist of passive elastic structures that are driven by oscillation and generate propulsion due to interactions between the elastic swimmer and fluid [17]. However, most artificial swimmers are incapable of bidirectional locomotion, which could enhance navigation in highly confined environments where turning is challenging, time-consuming, or infeasible.

Microorganisms have been observed to exhibit bidirectional propulsion. For instance, various bacterial species go through polymorphic modifications to use their flagellar appendages to propel forward and backward [18]. Additionally, sperm cells have reportedly been observed swimming backwards in the female reproductive system to fertilize an egg [18]. Inspired by these examples, recent studies have examined bidirectional propulsion for artificial swimmers. For instance, experimental work by Mohanty *et al.* [18] demonstrated arc-shaped magnetic swimmers with bidirectional locomotion using precessing magnetic fields in corkscrew-like actuation. They demonstrated bidirectional locomotion of the arc-shaped microswimmers, by taking advantage of the unique geometry to produce distinct dynamic conformations under precessing magnetic fields.

Likewise, theoretical works [19], [25] have shown that flexible oar swimmers with intrinsic curvature could exhibit bidirectional propulsion at low Re. For instance, work by Liu *et al.* [25] demonstrated a swimmer consisting of two symmetrically oriented elastic tails with circular arc profiles. The researchers found that varying curvatures can increase and reverse swimming direction. In another theoretical work, Liu *et al.* [19] demonstrated swimmers with circular arc and cosinusoidal profiles that could exhibit positive, negative, and bidirectional propulsion when actuated transversely at different frequencies at low Re. While the works presented bidirectional flexible oar swimmers, these findings have yet to be experimentally demonstrated.

Here, we experimentally demonstrate the bidirectional propulsion of flexible oar swimmers. We show intrinsically curved swimmers which are capable of positive, negative, and frequency-dependent bidirectional propulsion which could be utilized in highly confined environments. We also experimentally demonstrate that bidirectionality is curvature-dependent, suggesting that a single actuation frequency could be used for the independent control of multiple swimmers with varying curvatures. We envision the bidirectional intrinsically curved swimmers can be leveraged to increase the navigation versatility of microscale robots such as biomedical robots for targeted therapy and drug delivery.

## Methods

### Macroscopic experimental setup

To experimentally measure the propulsive force ⟨Fp⟩, experiments were performed in a glass tank (length: 1.20 m, width: 0.45 m) filled with high-viscosity silicone oil with a kinematic viscosity ($v$) of 100,000 cSt and a density ($\rho$) of 977 kg/m$^3$ (CAS # 63148-62-9, Clearco Products Co). The swimmer actuation assembly was attached to a load cell (108AA-100G, ANY LOAD) and suspended, so the actuated end of the swimmer was centered in width and depth (total silicone

depth: 34 cm), and 36.5 cm from the front wall (see Figure 1A). Force and frequency data were acquired using a data acquisition system (NI USB-6343). A camera (EOS R6, Canon) was rigidly mounted above the experiment to acquire swimmer deformation during experiments at 120 fps.

During experiments, swimmers were transversely actuated with frequencies from approximately 1.5 to 8.5 Hz, velocities (*U*) in the range of 94 to 315 mm/s, and swimmer lengths from 15 to 40 mm. Consequently, the Reynolds number ($Re = \rho UL/\mu$) in the experiment was in the range of 10 $e^{-1}$ to 10 $e^{-3}$, which adequately represents the low Re regime.

### Swimmer actuation

To actuate the swimmer during experiments, an assembly was designed which consisted of a 3D-printed housing, a geared DC motor (20.4:1 Metal Gearmotor 25Dx65L mm, Pololu) and Scotch Yoke mechanism to convert the motor's rotation into linear oscillations for transverse actuation of the swimmer. To control β, b was modified by controlling the distance between the disk pin and the disk center (Figure 1D)

### Swimmers

The swimmers in this work were 3D printed from photocurable clear resin (Clear Resin, FormLabs) with a layer resolution of 100 µm. After printing, swimmers were washed in isopropyl alcohol (IPA) for 20 min (Form Wash, FormLabs) and post-cured for 60 min at 60°C (Form Cure, FormLabs) following procedures in the material datasheet which reports the material's Young's modulus as E = 2.80 GPa. The rectangular swimmer cross-section was designed to yield in-plane bending during actuation.

Three swimmer profiles were used, namely straight (S), circular arc (C), and cosine (N1). Swimmers with C profiles consisted of a circular arc with a specific angle of curvature. For example, the C90 swimmer consisted of 90 degrees of a circular arc. Swimmers with N1 profiles consisted of one quarter of a cosine wave with an amplitude-to-wavelength ratio of α = 0.5. More specifically, the N1 profile was computed using the following equations from literature [19]:

$$y(s) = a\cos\frac{2\pi\tilde{x}(s)}{\lambda}, \quad \tilde{x} \in [0, N\lambda/4] \tag{1}$$

$$L = \frac{N\lambda}{2\pi}\int_0^{\pi/2}\sqrt{1+(2\pi\alpha\sin x)^2}\,dx \tag{2}$$

where α and λ denote the amplitude and wavelength of the cosine profile, respectively. The swimmer is composed of N quarter-waves, a uniform arclength $\tilde{s}$ and a contour length *L*. The bending stiffness is defined as $A = E^*I$, where *E* is the material Young's modulus and *I* is the second moment of area.

### Load *cell* and data acquisition

To measure Fp, a load cell was calibrated and used to attach the top part of the assembly to a rigid external frame (Figure 1B). An excitation voltage of +10 VDC (2231A-30-3 CAL DU, KEITHLEY) was applied across the circuit. The frequency dependent Fp was studied across a range of ω between approximately 1.5 Hz and 8.5 Hz which was controlled by modulating the input voltage of the geared DC motor. The data acquisition system and a custom LabVIEW program (National Instruments) were used to simultaneously acquire the Fp and ω.

## Data postprocessing

Experiment data were postprocessed using a custom MATLAB script to determine ⟨Fp⟩ and ⟨ω⟩. A second-order lowpass Butterworth filter was used to filter the force data to facilitate the identification of each period of oscillation. Preliminary experiments showed that steady-state motion was reached after approximately the first 50 periods of oscillation. Consequently, ⟨Fp⟩ and ⟨ω⟩ were determined in a window between the 100$^{th}$ oscillation and 110$^{th}$ oscillation. The time-averaged propulsive forces and frequencies for each experimental trial were computed as the mean values from the measurement window.

For each test condition, two independent experimental runs were performed to assess repeatability. Within each run, the script computed the mean and standard deviation of both ⟨Fp⟩ and ⟨ω⟩ across the ten steady-state cycles. These standard deviations quantify the variability in the force and frequency measurements and were used to estimate the percentage error for each condition. The reported ⟨Fp⟩ and ⟨ω⟩ values represent the mean of the two independent runs, while their corresponding standard deviations reflect the combined experimental uncertainty.

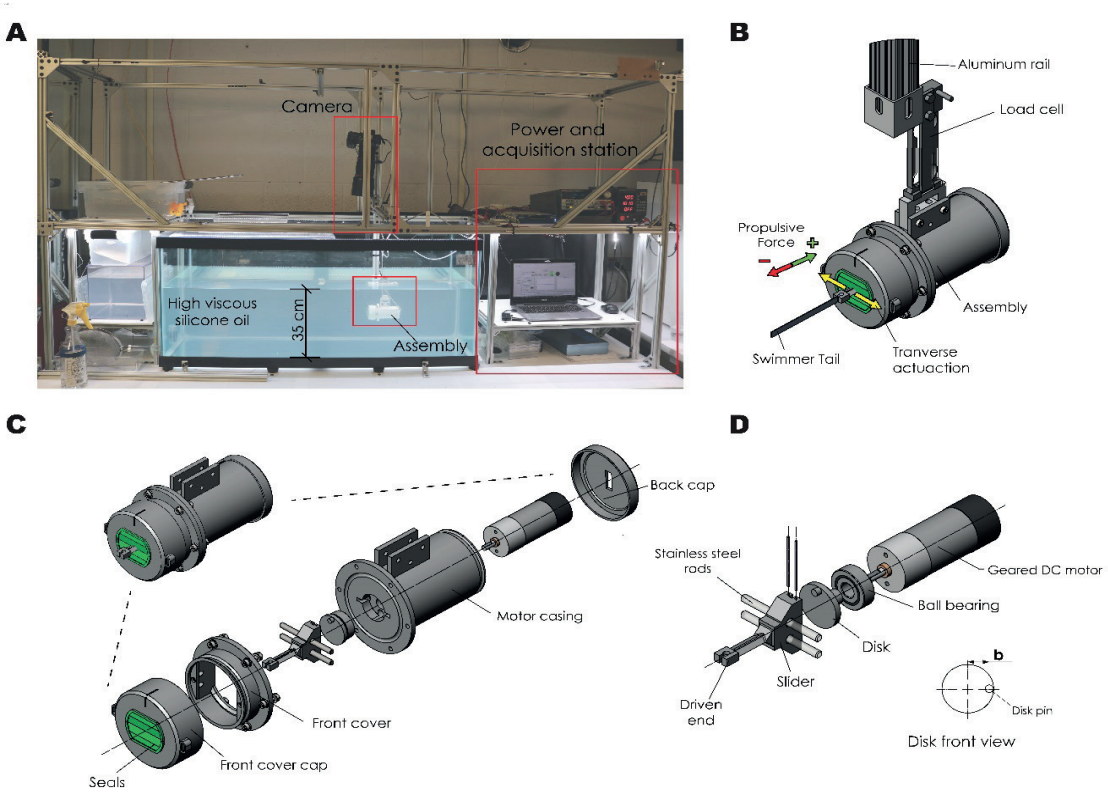


**Figure 1.** Experiment setup built to measure propulsion force of different swimmers. (A) Macroscopic setup comprised by the glass tank filled with silicone oil, assembly attached to the aluminum frame by the load cell, camera, and power and acquisition equipment. Assembly immersed half of the silicone oil height. (B) The actuation assembly and load cell to measure propulsive force. Indication of the propulsive force direction and swimmer's actuation. (C) Exploded view and components of the assembly. (D) Scotch yoke mechanism. The disk and slider from the Scotch yoke convert the motor's rotation into a linear movement. The actuation amplitude b is the half distance the filament's head will move back and forth.

## Results and discutions

### Swimmer's design and actuation

To experimentally study the bidirectional propulsion of flexible curved swimmers via the flexible oar swimming method, we designed swimmers with intrinsically-curved and straight profiles along the swimmer length. Two types of intrinsically-curved profiles, circular arc ("C90") and cosine ("N1"), were studied and compared to straight ("S") profiles. The C90 profile has a constant curvature that consists of 90 degrees of a circular arc, while the N1 profile has variable curvature that consists of one-quarter wavelength of a cosine curve, and amplitude to wavelength ratio (α) of 0.5. The swimmers, shown in Figure 2A, each have a contour length (L) of 22 mm and a rectangular cross-section with a height (h) of 5 mm and a thickness (t) of 0.5 mm.

Swimmers were experimentally tested with a macroscale setup in high viscosity silicone oil to achieve low Reynolds numbers between approximately 10 $\epsilon^{-1}$ and 10 $\epsilon^{-3}$. Swimmers were actuated by transverse oscillation at the leading edge, as shown in the inset in Figure 2Ai. The actuation frequency ⟨ω⟩ was adjusted to examine the frequency-dependent force, and the oscillation amplitude (b) was determined by the dimensionless variable β = b/L. During actuation, the flexible swimmer exhibited passive in-plane bending which induced a propulsive force due to traveling waves along the tail. [17] The propulsive force ⟨Fp⟩ and ω were simultaneous measured and used to determine the time-average propulsive force ⟨Fp⟩ and frequency ⟨ω⟩.

### Effect of swimmer profile on frequency-dependent propulsive force

To determine the effect of swimmer profile on bidirectional propulsion, we first determine the ⟨Fp⟩, calculated over ten consecutive oscillations (details in methods), when the swimmer is actuated between approximately 1.5 to 8.5 Hz (Figure 2B). A comparison of the data in Figure 2B shows that the propulsive force depends on swimmer profile. Indeed, the C90 and N1 profiles exhibit bidirectional propulsion with negative propulsion at low frequencies (C90: -0.80 ± 0.10 mN at 1.80 Hz, N1: -1.29 ± 0.11 mN at 1.71 Hz) and positive propulsion (C90: 2.90 ± 0.23 mN at 7.87 Hz, N1: 0.66 ± 0.19 mN at 7.41 Hz) at high frequencies. From the data, we estimate that bidirectionality occurs at approximately 3.0 Hz for the C90 swimmer and 6.0 Hz for the N1 swimmer. In comparison, the straight swimmer exhibits only positive forces, as expected from theory [19], [28]across the same frequency range. The bidirectional behavior observed for C90 and N1 is consistent with previous experimental and theoretical studies [18],[19],[25] showing that intrinsic curvature and the elastohydrodynamic response determine swimming direction when the actuation frequency crosses a critical value. Instantaneous profiles in Figure 2C enable visualization of the profile's deformation in one oscillation cycle. Mechanistically, at low ω the filament deforms quasi-statically and curvature-dominated strokes produce net rearward thrust; as ω increases the phase lag between base actuation and filament deformation grows and the filament adopts waveforms that are effectively forward-traveling, producing forward thrust. Those profile's deformations could be used in future studies to provide more insights into the relationship between the tail's deformation and bidirectionality.

### Effect of circular arc profile angle on bidirectionality

To further investigate the effect of intrinsic curvature on bidirectionality, experiments were performed with circular arc ("C") swimmers with angles of curvature between 0 and 180 degrees and the same contour length (L = 22 mm). The swimmers were transversely actuated (see Figure 3B) at three frequencies (1.5, 3.0, and 6.0 Hz) and β was fixed at 0.25, with two trials performed at each ω.

Results in Figure 3A reveal that the time-averaged propulsive force magnitude and direction can be affected by modifying the intrinsic curvature. At low curvature, swimmers exhibit only positive propulsion at the studied ω, whereas at higher curvatures (e.g., angle > 60 degrees), swimmer propulsive force tends to decrease. This finding aligns with an observation from literature, which indicates that increasing curvature reduces propulsive force and induces a lateral force that can change the direction of the total propulsive force [25]. The study also reports that the $\langle \overline{Fp} \rangle$ for an isolated flexible oar swimmer with circular cross-section actuated with angular oscillation reaches a local minimum at a nondimensional circular arc curvature ( $\overline{\kappa_c}$ ) of 2.5. Although our experimental results are for a single flexible oar swimmer with a rectangular cross-section actuated by transverse oscillation, results in Figure 3A show a similar finding at a lower $\overline{\kappa_c}$, as the results show a local minimum with the C120 swimmer, which has a $\overline{\kappa_c}$ of 2.1.Results in Figure 3A demonstrate that the C90, C120, and C150 swimmers exhibit bidirectional propulsion across the studied ω. C120 exhibits the lowest average negative force (-0.77 mN) at ω = 1.5 Hz. The force at the same ω is lower for C90 and C150 swimmers (C90: -0.37 mN, C150: -0.19 mN). At ω = 6.0 Hz, C120 has an average positive force of 1.42 mN, while the positive force values at 6.0 Hz are higher for C90 (1.80 mN) and C150 (1.60 mN). The previous observations indicate that bidirectional propulsion of swimmers with circular arc profiles can be enabled by adjusting swimmer curvature and actuation frequency.

Moreover, the existence of bidirectionality only beyond a threshold curvature (≈ 90° in our tests) agrees with the experimental observations of *Mohanty et al.* [20], who found that arc-shaped microswimmers driven by precessing magnetic fields require a minimum intrinsic curvature to produce propulsion reversal. Both their magnetic-actuation results and our mechanically actuated swimmers indicate that curvature not only breaks fore–aft symmetry but also tunes the relative weight of elastic and viscous timescales that determine the sign of propulsion.

Finally, our findings suggest that intrinsic curvature modulates both the magnitude and the direction of propulsion, with an optimal curvature range ($\bar{\kappa}c \approx 2 – 2.5$) where hydrodynamic and elastic effects balance to yield bidirectionality, consistent with theoretical predictions *[19],[25]* and experimental demonstrations. [18]

### Effect of the actuation amplitude on propulsive force

To examine the effect of oscillation amplitude on propulsive force magnitude and direction, experiments were performed at β = 0.10, 0.25, and 0.45. Studying the effect of oscillation amplitude on propulsive force is desirable because higher amplitudes have been shown in prior literature to enhance the propulsion force and locomotion[19]-[25] In each experiment, “b” was modified in the experimental setup (details in Figure 1D) to enable tests at β = 0.10, 0.25, and 0.45. Swimmers with S, C90, and N1 profiles and identical dimensions (L = 22 mm, h = 5 mm, t = 0.5 mm) were actuated in two trials in a frequency range between 1.5 Hz and 8.5 Hz.

First, we analyze the time-averaged propulsive force as a function of the actuation frequency for S, C90, and N1 swimmers (Figure 4B). The experiment results reveal that the magnitude of propulsive force increases with increasing β, suggesting that the force response of swimmers can be improved by increasing actuation amplitude. Indeed, results in Figure 4C demonstrate that the propulsive force scales with $\beta^2$, as shown in several other studies.[19]-[25]

Pak and Lauga [29] analytically demonstrated that for small-amplitude periodic deformations, the leading-order propulsion speed scales with the square of the actuation amplitude, as a consequence of the nonlinear coupling between shape and flow field required to break time-reversible motion at low Reynolds number. Similarly, Gazzola *et al.* [30] used direct numerical simulations to show that increasing the nondimensional actuation amplitude leads to a quadratic increase in both propulsive force and swimming efficiency, up to a saturation regime where large-amplitude effects become significant. Experimental work by Qiu *et al.* [1]

on magnetically actuated flexible microswimmers confirmed that the time-averaged propulsive thrust is proportional to $\beta^2$ over a broad range of actuation frequencies, thus validating this scaling law experimentally. The N1-22 data in Figure 4C iii indicate that the frequencies at which bidirectionality occurs can differ depending on β. For example, N1-22 exhibits bidirectionality at approximately 6.0 Hz at β = 0.25, and data suggest that bidirectionality could occur at approximately 7.0 Hz at β = 0.45.

The C90-22 data, on the other hand, show bidirectionality at the same approximate ⟨ω⟩ (3.0 Hz), suggesting that the bidirectionality frequency of swimmers with circular arc profiles could be unaffected by actuation amplitude, though further studies are needed to verify this hypothesis. We also note that the β = 0.1 tests exhibited larger standard deviations which are likely due to the relatively lower signal-to-noise ratio from the small propulsive forces at β = 0.1. The relatively lower forces and higher amount of error in β = 0.1 complicate data interpretation and suggest that low oscillation amplitudes could negatively affect swimmer performance in practice.

Figure 4D shows instantaneous profiles for each swimmer at each β. Overall, we observe that the swimmers exhibit higher deformation at higher β, resulting in greater propulsive force. Further work is needed to understand the relationship between instantaneous profiles and propulsive force. We anticipate that a greater understanding of the relationship between instantaneous profile and force could yield additional insights for further enhancing bidirectional propulsion.

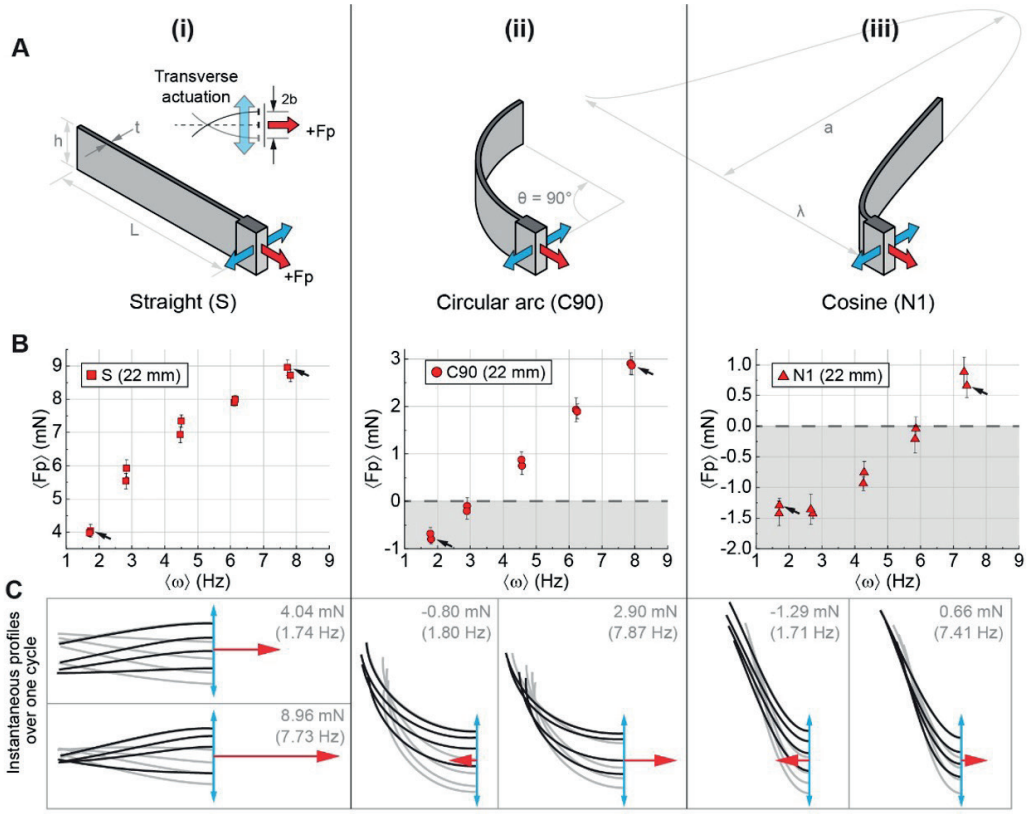


**Figure 2.** Effect of swimmer profile on frequency-dependent propulsive force. (A) Three-dimensional illustrations of swimmers with straight "S" (i), circular arc "C90" (ii), and cosine "N1" (iii) profiles and the same contour length (L = 22 mm), height (h = 5 mm), and thickness (t = 0.5 mm). Inset in (Ai) shows a top view of transverse actuation (blue arrows), which causes the swimmer to flex and generate a propulsive force (Fp, red arrows). (B) Frequency-dependent time-averaged propulsive force ⟨Fp⟩ of swimmers shown in (A). Comparison between swimmers shows the effect of intrinsic curvature (κ) on the direction and magnitude of the propulsive force at low Re. Bidirectional propulsion can be achieved by the N1 and C90 swimmers by modulating ⟨ω⟩. (C) Instantaneous swimmer profiles showing deformation in one cycle of tests indicated by black arrows in (B). Black and gray profiles show the deformation in an upward and downward stroke, respectively. Red arrows are scaled to represent the force magnitude and direction, and blue arrows indicate the transverse actuation direction. Text labels report ⟨Fp⟩ and ⟨ω⟩.

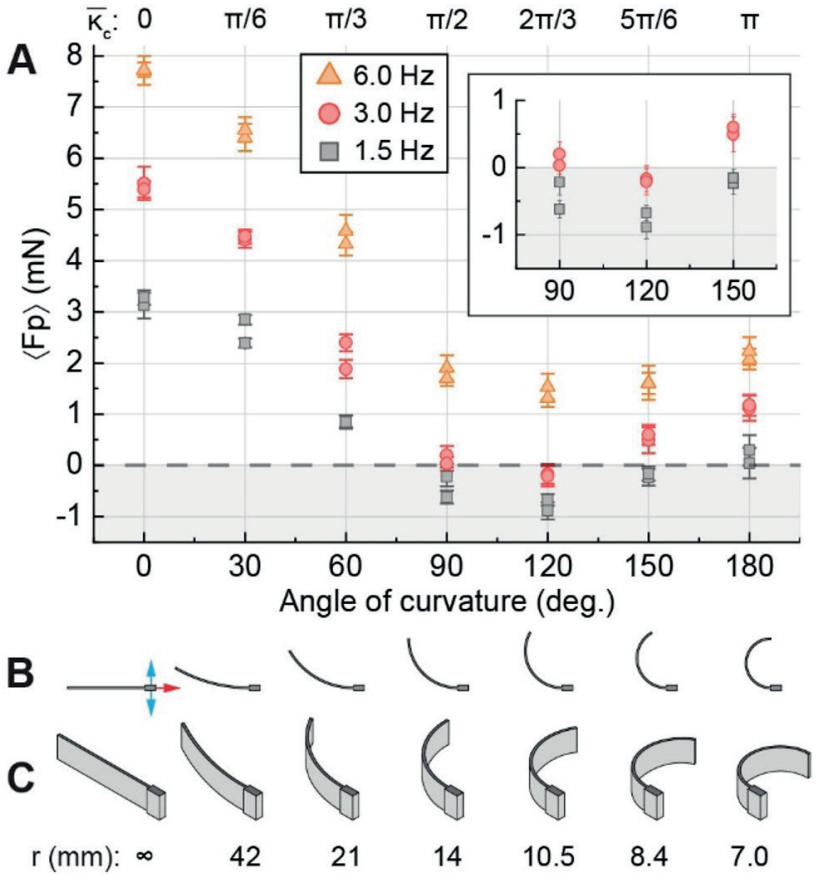


**Figure 3.** Effect of circular arc curvature on bidirectionality. (A) Frequency-dependent propulsive force as a function of curvature angle for C swimmers with L = 22 mm, h = 5 mm, and t = 0.5 mm. Swimmers were oscillated at three actuation frequencies, with β = 0.25. Error bars show the standard deviation within each experimental trial. Inset shows the swimmers exhibiting bidirectional propulsion. Labels above plot report the nondimensional curvature ( $\overline{\kappa_c}$ ) for each swimmer. (B-C) Top and isometric views of each swimmer with transverse actuation (blue arrows) and positive direction of propulsive force (red arrows) indicated on the "C0" swimmer which has a straight profile.

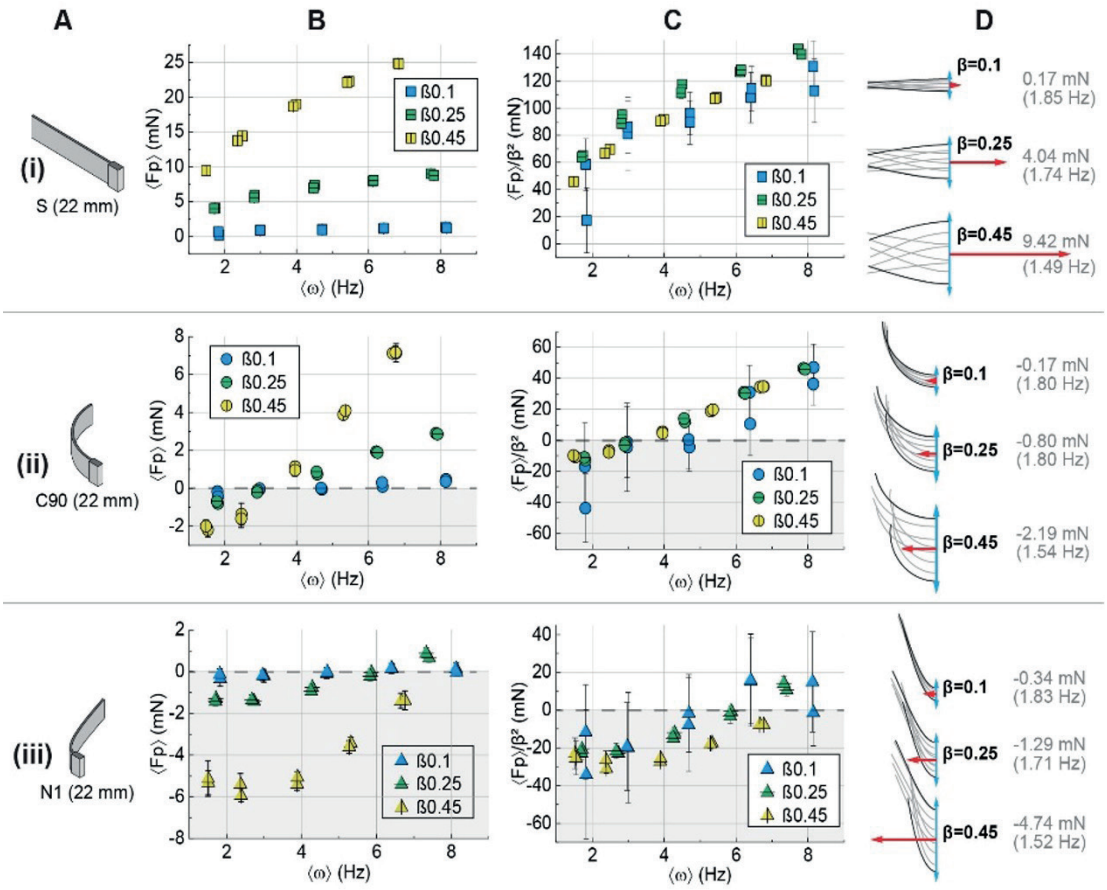


**Figure 4.** Effect of oscillation amplitude on propulsive force. (A) Three-dimensional illustrations of swimmers with S (i), C90 (ii), and N1(iii) profiles and L = 22 mm. (B) ⟨Fp⟩ for swimmers actuated at three scaled oscillation amplitudes (β = 0.1, 0.25, and 0.45). (C) ⟨Fp⟩ data from (B) scaled by $\beta^2$. (D) Instantaneous profiles during one cycle at low frequency for each β, with red arrows scaled to denote the force magnitude and direction. Black lines indicate the profile at the bounds of the oscillation. Text labels report ⟨Fp⟩ and ⟨ω⟩ for the drawn profiles.

## Conclusions

The ability to control microswimmers in the low-Reynolds-number regime opens new frontiers in biomedical engineering, enabling access to previously unreachable regions within the human body for applications such as targeted drug delivery, minimally invasive microsurgery, and localized diagnostics. However, conventional flexible oar microswimmers typically exhibit unidirectional propulsion, limiting their navigation capabilities in confined or complex environments.

In this study, we experimentally demonstrated a class of intrinsically curved flexible oar microswimmers capable of bidirectional propulsion at low Reynolds numbers. The combined results from Figures 2–4 revealed that the propulsion direction and magnitude are governed by the interplay between geometry, actuation frequency, and oscillation amplitude. Introducing intrinsic curvature enables swimmers to achieve positive, negative, and frequency-dependent propulsion, allowing directional reversal without reorientation—a key advantage for operation in microvasculature or tissue channels where turning is infeasible. Moreover, the propulsive force

was shown to scale with the square of the actuation amplitude ($\beta^2$), consistent with theoretical [29], numerical [30], and experimental [1] studies, confirming that nonlinear coupling between deformation and viscous stresses governs locomotion at low Re.

Despite these promising findings, some experimental limitations should be acknowledged. The experiments were performed in simplified laboratory fluids that do not fully capture the viscoelastic or heterogeneous properties of biological media. The force sensitivity at small oscillation amplitudes ($\beta \approx 0.1$) introduced higher uncertainty in measurements, and potential boundary effects from the tank walls may have influenced the local hydrodynamics. Furthermore, the planar actuation constraint restricted investigation of three-dimensional swimming behaviors that may emerge in free or helical motion. Addressing these limitations will require future studies with improved force resolution, reduced boundary interference, and actuation schemes capable of exploring fully 3D kinematics.

The demonstrated bidirectional propulsion mechanism has important real-world implications. Microswimmers with reversible motion could enhance next-generation microrobotic systems for targeted therapy, minimally invasive surgery, and precision diagnostics. Prior research has established the feasibility of microrobotic propulsion for biomedical use—ranging from biomimetic surgical micro-robots [3], sperm-driven and flagellar microrobots [5], [6], and artificial bacterial flagella for single-cell drug delivery [7], to magnetically guided microrobots for targeted delivery and imaging [8], [9]. Integrating the intrinsic-curvature design with magnetic or acoustic actuation could enable controllable, reversible motion in complex fluidic or biological networks, improving navigation efficiency and reducing the need for external mechanical reorientation.

Ultimately, the introduction of intrinsic curvature as a mechanism for bidirectional propulsion marks a step toward a new class of adaptive microswimmers capable of intelligent navigation in complex microenvironments. Future research should bridge the gap between fundamental mechanics and clinical translation by (i) testing swimmer performance in biologically relevant fluids, (ii) integrating autonomous control via external fields or onboard sensing, and (iii) exploring collective behaviors for swarm-based transport. These advances could lead to functional microrobots capable of operating within living systems—realizing the long-standing vision of controllable, minimally invasive microscale machines for precision medicine.

## References

[1] T. Qiu, T. C. Lee, A. G. Mark, K. I. Morozov, R. Münster, O. Mierka, S. Turek, A. M. Leshansky, and P. Fischer, “Swimming by reciprocal motion at low Reynolds number,” *Nat. Commun.*, vol. 5, 2014.

[2] M. Jabbarzadeh, “Hydrodynamic interactions and motion of bacteria at low Reynolds number,” Ph.D. dissertation, Dept. Math., Univ. of Utah, Salt Lake City, UT, USA, 2018.

[3] J. Edd, S. Payen, B. Rubinsky, M. L. Stoller, and M. Sitti, “Biomimetic propulsion mechanism for a swimming surgical micro-robot,” in *Proc. IEEE/RSJ Int. Conf. Intell. Robot. Syst. (IROS)*, vol. 3, pp. 2583–2588, 2003.

[4] V. Magdanz *et al.*, “IRON Sperm: Sperm-templated soft magnetic microrobots,” *Sci. Adv.*, vol. 6, no. 28, 2020.

[5] A. V. Singh *et al.*, “Sperm cell driven microrobots—Emerging opportunities and challenges for biologically inspired robotic design,” *Micromachines*, vol. 11, no. 4, 2020.

[6] G. Kósa *et al.*, “Flagellar swimming for medical micro robots: Theory, experiments and application,” in *Proc. IEEE/RAS-EMBS Int. Conf. Biomed. Robot. Biomechatronics (BioRob)*, pp. 258–263, 2008.

[7] R. Mhanna *et al.*, “Artificial bacterial flagella for remote-controlled targeted single-cell drug delivery,” *Small*, vol. 10, no. 10, pp. 1953–1957, 2014.

[8] I. S. M. Khalil *et al.*, “Magnetic control of potential microrobotic drug delivery systems: Nanoparticles, magnetotactic bacteria and self-propelled microjets,” in *Proc. Annu. Int. Conf. IEEE Eng. Med. Biol. Soc. (EMBS)*, pp. 5299–5302, 2013.

[9] K. T. Nguyen *et al.*, “A magnetically guided self-rolled microrobot for targeted drug delivery, real-time X-ray imaging, and microrobot retrieval,” *Adv. Healthc. Mater.*, vol. 10, no. 6, 2021.

[10] S. Fusco *et al.*, "Shape-switching microrobots for medical applications: The influence of shape in drug delivery and locomotion," *ACS Appl. Mater. Interfaces*, vol. 7, no. 12, pp. 6803–6811, 2015.

[11] D. Jang, J. Jeong, H. Song, and S. K. Chung, "Targeted drug delivery technology using untethered microrobots: A review," *J. Micromech. Microeng.*, vol. 29, no. 5, 2019.

[12] G. Chatzipirpiridis *et al.*, "Electroforming of implantable tubular magnetic microrobots for wireless ophthalmologic applications," *Adv. Healthc. Mater.*, vol. 4, no. 2, pp. 209–214, 2015.

[13] F. Ullrich *et al.*, "Mobility experiments with microrobots for minimally invasive intraocular surgery," *Invest. Ophthalmol. Vis. Sci.*, vol. 54, no. 5, pp. 2853–2863, 2013.

[14] Z. Ren *et al.*, "Soft-bodied adaptive multimodal locomotion strategies in fluid-filled confined spaces," *Sci. Adv.*, vol. 7, no. 24, 2021.

[15] H. W. Huang *et al.*, "Adaptive locomotion of artificial microswimmers," *Sci. Adv.*, vol. 5, no. 1, 2019.

[16] J. Lighthill, "Flagellar hydrodynamics," *SIAM Rev.*, vol. 18, no. 2, pp. 161–230, 1976.

[17] E. M. Purcell, "Life at low Reynolds number," *Am. J. Phys.*, vol. 45, no. 1, pp. 3–11, 1977.

[18] S. Mohanty *et al.*, "Bidirectional propulsion of arc-shaped microswimmers driven by precessing magnetic fields," *Adv. Intell. Syst.*, vol. 2, no. 7, 2000064, 2020.

[19] Z. Liu, F. Qin, and L. Zhu, "Actuating a curved elastic filament for bidirectional propulsion," *Phys. Rev. Fluids*, vol. 5, no. 5, 2020.

[20] C. H. Wiggins and R. E. Goldstein, "Flexive and propulsive dynamics of elastica at low Reynolds number," *Phys. Rev. Lett.*, vol. 80, no. 17, pp. 3879–3882, 1998.

[21] E. Lauga, "Floppy swimming: Viscous locomotion of actuated elastica," *Phys. Rev. E*, vol. 75, no. 4, 2007.

[22] T. S. Singh, P. Singh, and R. D. S. Yadava, "Effect of interfilament hydrodynamic interaction on swimming performance of two-filament microswimmers," *Soft Matter*, vol. 14, no. 19, pp. 7748–7757, 2018.

[23] W. H. Zurek, "Sub-Planck structure in phase space and its relevance for quantum decoherence," *New J. Phys.*, vol. 2, no. 10, 2000.

[24] Z. Peng, G. J. Elfring, and O. S. Pak, "Maximizing propulsive thrust of a driven filament at low Reynolds number via variable flexibility," *Soft Matter*, vol. 13, no. 12, pp. 2339–2346, 2017.

[25] Z. Liu, F. Qin, L. Zhu, R. Yang, and X. Luo, "Effects of the intrinsic curvature of elastic filaments on the propulsion of a flagellated microrobot," *Phys. Fluids*, vol. 32, no. 7, 2020.

[26] O. S. Pak and E. Lauga, "Theoretical models in low-Reynolds-number locomotion," *Soft Matter*, vol. 10, no. 1, pp. 401–414, 2014.

[27] R. Dreyfus, J. Baudry, M. L. Roper, M. Fermigier, and H. A. Stone, "Microscopic artificial swimmers," *Nature*, vol. 437, pp. 862–865, 2005.

[28] T. S. Yu, E. Lauga, and A. E. Hosoi, "Experimental investigations of elastic tail propulsion at low Reynolds number," *Phys. Fluids*, vol. 18, no. 9, 2006.

[29] O. S. Pak and E. Lauga, "Generalized squirming motion of a sphere," *Journal of Engineering Mathematics*, vol. 88, no. 1, pp. 1–28, 2014.

[30] M. Gazzola, M. Argentina, and L. Mahadevan, "Gait and speed selection in slender inertial swimmers," *Proceedings of the National Academy of Sciences of the United States of America (PNAS)*, vol. 111, no. 36, pp. 13695–13700, 2014.

## Declaración sobre uso de Inteligencia Artificial (IA)

Para la revisión gramatical y ortográfica de este artículo, empleamos la herramienta de IA *ChatGPT*. Esta nos permitió identificar errores y mejorar la fluidez del texto. No obstante, realizamos una revisión final para garantizar que el artículo cumpliera con los estándares de calidad de la revista..